Calculating vibrational excited state absorptions with excited state constrained minimized energy surfaces

Yiwen Wang, Zehua Chen, and Yang Yang*

Theoretical Chemistry Institute and Department of Chemistry, University of Wisconsin-Madison, 1101 University Avenue, Madison, Wisconsin 53706, United States

E-mail: yyang222@wisc.edu

Abstract

The modeling and interpretation of vibrational spectra are crucial for studying reaction dynamics using vibrational spectroscopy. Most prior theoretical developments focused on describing fundamental vibrational transitions while fewer developments focused on vibrational excited state absorptions. In this study, we present a new method that uses excited state constrained minimized energy surfaces (CMES) to describe vibrational excited state absorptions. The excited state CMESs are obtained similarly to the previous ground state CMES development in our group but with additional wave function orthogonality constraints. Using a series of model systems, including the harmonic oscillator, Morse potential, double-well potential, quartic potential, and two-dimensional anharmonic potential, we demonstrate that this new procedure provides good estimations of the transition frequencies for vibrational excited state absorptions. These results are significantly better than those obtained from harmonic approximations using conventional potential energy surfaces, demonstrating the promise of excited state CMES-based methods for calculating vibrational excited state absorptions in real systems.

Introduction

Vibrational spectroscopy is a powerful tool for obtaining structural information and uncovering reaction dynamics in both the gas and condensed phases ^{1–5}. Compared to conventional linear vibrational spectroscopy, nonlinear vibrational spectroscopy can provide additional information by probing two or more photon processes ^{6–11}. For example, two-dimensional infrared spectroscopy (2DIR) can go beyond the vibrational ground state and monitor the vibrational excited state dynamics and thus has been used to investigate reaction dynamics in a variety of materials and biological systems ^{12–17}.

There have been many theoretical methods to model vibrational spectroscopy. The most widely used method to estimate vibrational frequencies is to diagonalize the mass-weighted Hessian matrices obtained from either density functional theory (DFT) or wave function theories ¹⁸. This method invokes the harmonic approximation and can generally provide qualitatively correct vibrational mode results; however, when describing systems with strong anharmonicities, it often relies on empirical scaling factors to obtain quantitatively correct results ¹⁹. Going beyond the harmonic approximation, vibrational second order perturbation theory (VPT2) ^{20–24} is often used to obtain anharmonicity-corrected vibrational frequencies, which utilizes information from local higher-order derivatives. VPT2 has good balance between accuracy and efficiency, although it may face challenges when local higher-order derivatives are not sufficient to capture the behavior of the whole potential energy surface (PES), especially in some shared proton systems with double-well PESs ^{25–31}. Vibrational self-consistent field theory (VSCF) ³² is currently one of the most accurate methods for obtaining vibrational spectra. It utilizes a high-dimensional PES to compute vibrational ground and excited states. By using the n-mode representation of the potential ³³, the VSCF and VCI methods have been applied to molecules and clusters with 10 or more atoms ^{34,35}.

In addition to the aforementioned popular methods based on static calculations, another category of methods is based on dynamic simulations and employs time autocorrelation functions to obtain vibrational spectra. Among them, a widely-used method is classical molecular dynamics (MD)^{36–38}, which treats nuclei as classical particles and evolves them classically on PESs following Newton's laws of motion. Within the classical MD framework, ab initio MD (AIMD) is generally more accurate than force-field-based MD because the PESs used in AIMD are obtained through ab initio electronic structure calculations, such as DFT. However, classical MD can only take into account a limited amount of anharmonicty through dynamic simultations on PESs at a finite temperature and often needs empirical scaling factors for highly anharmonic systems. An improved way to incorporate anharmonicity in MD simulations is through quasi- or semi- classical methods^{39–43}. These methods assign certain initial energies to the nuclei, and thus the resulting classical trajectories can reach more anharmonic areas of the PES. This treatment is successful in many model and practical

systems, although it can suffer from zero-point energy (ZPE) leakage problems in some systems 44,45. A more elegant way of incorporating anharmonicity in MD simulations is through the path-integral formulism. A few major variants are centroid molecular dynamics (CMD)^{46,47}, ring-polymer molecular dynamics (RPMD)⁴⁸, thermostated ring-polymer molecular dynamics (TRPMD)⁴⁹, and quasi-centroid molecular dynamics (QCMD)⁵⁰. The theoretical foundation of the path-integral methods is the quantum-classical isomorphism, which can map a quantum system onto a classical system with chains of beads⁵¹. These beads evolve classically on a PES, and the bead distribution connects with the quantum probability density, thus describing nuclear quantum effects. As such, these path-integral methods can describe anharmonicity and provide relatively accurate vibrational spectra through reasonable approximations to the time autocorrelation functions ^{51–53}. An even more accurate method to describe vibrational spectra is through quantum nuclear dynamics, and a commonlyused method is the multiconfigurational time-dependent Hartree (MCTDH) theory ^{54–57}. Although the underlying computational cost remains a major limiting factor, this theory has been shown to accurately describe the vibrational spectra of systems as large as water clusters with four water molecules ⁵⁸.

In the past few years, our group has developed a new method for calculating vibrational spectra based on constrained minimized energy surfaces (CMESs)⁵⁹. The CMES is an effective PES for nuclei, but compared to the conventional PES, the CMES incorporates nuclear quantum effects, especially the zero-point effects, in the effective potential energy surface. It has been shown with a few model systems that MD based on the CMES (CMES-MD) is able to give significantly more accurate fundamental vibrational frequencies than conventional MD, and its performance is comparable to or even better than CMD and RPMD⁵⁹. In real molecular systems, our group has developed constrained nuclear-electronic orbital density functional theory (CNEO-DFT)⁶⁰⁻⁶² to approximate the CMES. It was found that CNEO-DFT harmonic frequencies are already comparable to or better than VPT2⁶², and the vibrational spectra obtained from MD simulations on CNEO-DFT

energy surfaces accurately reproduce the experimental spectra 63 . Despite this success, these past developments were mostly focused on the fundamental $0 \to 1$ excitations. In order to simulate nonlinear vibrational spectra, especially the $1 \to 2$ excitations, a method that can describe vibrational excited state absorptions is essential. One example of the importance of describing these excitations is in 2D-IR spectra, where the $0 \to 1$ fundamental transitions appear on the diagonal line, whereas the $1 \to 2$ excited state absorptions can be observed next to them but slightly off the diagonal line, together forming the butterfly-shaped feature of the spectra 12 .

For the excited state absorptions, conventional MD cannot distinguish them from fundamental transitions since the underlying theoretical foundation for spectra calculations using MD is a harmonic approximation 64 , in which the fundamental $0 \to 1$ excitation and all excited state $n \to n+1$ transitions share the same transition energy. Quasi- or semi-classical methods can possibly describe these excited state absorptions by giving more initial energy to the nuclei 40,41. However, their ZPE leakage problems 44,65 could become more severe because of the even higher initial energy given to the systems. Currently, a commonly used method for describing the vibrational excited state absorptions in the 2DIR spectrum is to first obtain the PES for the mode of interest while fixing all other modes ^{66–70}, and then either fit the PES to a Morse potential and approximate the results with the exact quantum solutions for the Morse potential⁶⁶, or utilize the discrete variable representation (DVR) method to solve the Schrödinger equation with a careful choice of modes to be coupled ⁶⁹. These methods have been successfully applied to a series of systems and provided important physical insights ^{26,66,69–74}. One drawback of these methods is that their accuracy is often sensitive to what modes and how many modes are allowed to couple in the calculation, which means that empirical knowledge is often needed. As such, these methods may face great challenges in systems with a complex coupling picture ⁷¹. Therefore, it remains highly desirable to develop a method that can accurately and efficiently simulate vibrational excited state absorptions in a relatively black-box manner.

In this paper, we propose a new way of calculating vibrational excited state absorptions by constructing excited state CMESs and using their second-order derivative information to approximate the vibrational transition energies. This is essentially equivalent to performing MD simulations at the zero-temperature limit. We systematically test the new method on a series of model systems and benchmark the results against the exact quantum references. We will show that the results are significantly better than the harmonic approximation results based on the ground state PES. This paper will serve as the theoretical foundation for our future development and utilization of excited state CNEO theory to calculate vibrational excited state absorptions in real molecular systems.

Theory

Ground state CMES

Although this paper will focus on developing excited state CMES theory, here we provide a brief review of the ground state CMES theory so that the development of excited state CMES theory can follow naturally. The CMES-MD framework was recently developed in our group as an alternative approach to incorporate nuclear quantum effects in MD simulations 59 . In conventional PES-based MD simulations, nuclei are treated as classical point charges, which ignores the quantum delocalization of the nuclei. In contrast, in CMES-MD, nuclei are treated quantum mechanically, but instead of directly evolving the quantum nuclei according to the time-dependent Schrödinger equation, an adiabatic approximation is invoked where for every point in phase space with specified nuclear expectation positions and nuclear expectation momenta (\mathbf{X}, \mathbf{P}) that the system evolves to, the system immediately relaxes to the energy-minimized quantum state with the same nuclear expectation positions and momenta $(\mathbf{X}, \mathbf{P})^{59}$. Under this assumption, it can be proven that the nuclear expectation positions and expectation momenta evolve classically according to Newton's laws of motion on the effective potential energy surface, i.e., the CMES, instead of the conventional PES 59 .

As such, the CMES method can be viewed as an alternative formulation or approximation to the Ehrenfest theorem.

A key to performing CMES-MD is to construct the CMES, which is a function of nuclear expectation positions and can be obtained by searching for the lowest-energy nuclear wave function that satisfies the nuclear expectation position constraint:

$$V_0^{\text{CMES}}(\mathbf{X}) = \min_{A_0 \in \mathscr{H}_0^{\text{sub}}} \langle A_0 | \hat{H} | A_0 \rangle, \quad \mathscr{H}_0^{\text{sub}} = \{ A \in \mathscr{H} | \langle A | \hat{\mathbf{x}} | A \rangle = \mathbf{X} \}$$
 (1)

Here \mathscr{H} is the quantum nuclear Hilbert space and $\mathscr{H}_0^{\mathrm{sub}}$ is a subspace that satisfies the nuclear expectation constraint, $\langle A|\hat{\boldsymbol{x}}|A\rangle=\mathbf{X}$. This constrained minimization can be performed using the Lagrangian function:

$$\mathcal{L} = \langle A_0 | \hat{H} | A_0 \rangle + \mathbf{f}_0 \cdot (\langle A_0 | \hat{\mathbf{x}} | A_0 \rangle - \mathbf{X}) - \tilde{E}_0 (\langle A_0 | A_0 \rangle - 1)$$
(2)

in which f_0 is the Lagrange multiplier associated with the expectation position constraint, and \tilde{E}_0 is the Lagrange multiplier associated with the wave function normalization constraint. Making the Lagrangian function stationary by varying the state $|A_0\rangle$ leads to an eigenvalue equation

$$[\hat{H} + \mathbf{f}_0 \cdot \hat{\mathbf{x}}] |A_0\rangle = \tilde{E}_0 |A_0\rangle. \tag{3}$$

This eigenvalue equation can be solved iteratively together with the expectation constraint as well as the normalization constraint, leading to solutions of $f_0(\mathbf{X})$, $|A_0(\mathbf{X})\rangle$, and $\tilde{E}_0(\mathbf{X})$, which are all functions of the quantum nuclear expectation position ⁵⁹. When the constraints are satisfied, the total energy, which is a function of the nuclear expectation positions, will serve as the effective PES, or the CMES:

$$V_0^{\text{CMES}}(\mathbf{X}) = \langle A_0(\mathbf{X}) | \hat{H} | A_0(\mathbf{X}) \rangle \tag{4}$$

The nuclear expectation positions and momenta evolve according to the Newtonian equations⁵⁹

$$\frac{\mathrm{d}\langle \hat{\boldsymbol{x}} \rangle}{\mathrm{d}t} = \frac{\langle \hat{\boldsymbol{p}} \rangle}{m} \tag{5}$$

$$\frac{\mathrm{d}\langle \hat{\boldsymbol{p}} \rangle}{\mathrm{d}t} \approx -\nabla_{\mathbf{X}} V_0^{\mathrm{CMES}}(\mathbf{X}) \tag{6}$$

Note that the evolution of momenta is not exact since we have invoked the adiabatic approximation and assumed that the system immediately relaxes to the energy-minimized quantum state for a given nuclear expectation position X^{59} . Based on these working equations, CMES-MD can be performed, and our group has demonstrated that CMES-MD trajectories lead to accurate vibrational spectra in both model systems and practical molecular systems 59,63 .

The theoretical justification for simulating vibrational spectra based on classical MD simulations, including both conventional MD and CMES-MD, is based on two factors. First, according to Fermi's Golden Rule⁷⁵, the Fourier spectrum of quantum autocorrelation functions can be used to calculate transition frequencies and intensities between energy levels. Second, in the harmonic oscillator model, the classical and quantum autocorrelation functions yield identical peak positions, differing only by a prefactor in intensities ⁶⁴. Although this harmonic approximation enables vibrational spectra to be calculated from classical MD simulations, it also leads to the assumption that the fundamental excitations $(0 \to 1)$ are the same in energy as those from excited state absorptions (e.g. $1 \to 2$, $2 \to 3$). However, in anharmonic systems, there are slight differences among these absorption energies, which can be observed, for example, in 2DIR experiments. We note that although it has been observed that increasing the simulation temperature in MD simulations results in redshifts, which might be viewed as an incorporation of some excited state absorptions, there is no solid theoretical foundation for this temperature effect, which is an artifact from classical treatments⁷⁶.

Excited states CMES

Here we propose a new way of separately obtaining excited state and ground state absorption frequencies by constructing and using excited state CMESs.

Previously in developing the CMES theory, our group has targeted the eigenstate with the lowest energy. These states are essentially the ground states that satisfy the expectation constraints. However, there are also "excited states" with higher energies. To search for these excited states for a given nuclear expectation position, we can perform constrained energy minimization again. The first excited state CMES can be defined as

$$V_1^{\text{CMES}}(\mathbf{X}) = \min_{A_1 \in \mathcal{H}_1^{\text{sub}}} \langle A_1 | \hat{H} | A_1 \rangle, \quad \mathcal{H}_1^{\text{sub}} = \{ A \in \mathcal{H} | \langle A | \hat{x} | A \rangle = \mathbf{X}, \langle A | A_0(\mathbf{X}) \rangle = 0 \}, \quad (7)$$

where $\mathscr{H}_1^{\text{sub}}$ is another subspace of the Hilbert space \mathscr{H} in which the states satisfy not only the expectation position constraint, but also the orthogonality constraint to the CMES ground state with the same expectation position, i.e., $\langle A_1(\mathbf{X})|A_0(\mathbf{X})\rangle = 0$. Following the same logic, a more general definition for the *n*th excited state CMES can be defined as

$$V_n^{\text{CMES}}(\mathbf{X}) = \min_{A_n \in \mathcal{H}_n^{\text{sub}}} \langle A_n | \hat{H} | A_n \rangle, \quad \mathcal{H}_n^{\text{sub}} = \{ A \in \mathcal{H} | \langle A | \hat{\boldsymbol{x}} | A \rangle = \mathbf{X}, \langle A | A_i(\mathbf{X}) \rangle = 0, \forall i = 0, 1, \cdots, n-1 \},$$
(8)

in which we required the nth excited constrained minimized energy state to be orthogonal to all the lower-energy states with the same expectation position. Under these constraints, the Lagrangian function for solving the nth excited state CMES can be written as

$$\mathcal{L} = \langle A_n | \hat{H} | A_n \rangle + \mathbf{f}_n \cdot (\langle A_n | \hat{\mathbf{x}} | A_n \rangle - \mathbf{X}) + \sum_{i=0}^{n-1} g_{ni} \cdot \left| \langle A_n | A_i(\mathbf{X}) \rangle \right|^2 - \tilde{E}_n(\langle A_n | A_n \rangle - 1), \quad (9)$$

where g_{ni} is the Lagrange multiplier associated with the orthogonality constraint to the *i*th CMES state $A_i(\mathbf{X})$. Note that to facilitate subsequent derivations and practical implementations, here we employed the constraint as $\left|\langle A_n|A_i(\mathbf{X})\rangle\right|^2=0$ instead of the simple form of $\langle A_n|A_i(\mathbf{X})\rangle=0$. Making the Lagrangian function stationary by varying A_n can lead to the eigenvalue

equation for solving the nth excited CMES state:

$$\left(\hat{H} + \boldsymbol{f}_n \cdot \hat{\boldsymbol{x}} + \sum_{i=0}^{n-1} g_{ni} \cdot |A_i(\mathbf{X})\rangle \langle A_i(\mathbf{X})|\right) |A_n(\mathbf{X})\rangle = \tilde{E}_n(\mathbf{X})|A_n(\mathbf{X})\rangle.$$
(10)

When all lower states $A_i(\mathbf{X})$ are known, this eigenvalue equation can be solved iteratively together with the expectation constraint, the normalization constraint, and the orthogonality constraints, and we will obtain solutions of $\mathbf{f}_n(\mathbf{X})$, $g_{ni}(\mathbf{X})$, $|A_n(\mathbf{X})\rangle$, and $\tilde{E}_n(\mathbf{X})$, which are all functions of the nuclear expectation positions. When all constraints are satisfied, the total energy will serve as the effective PES for the *n*th excited constrained minimized energy state:

$$V_n^{\text{CMES}}(\mathbf{X}) = \langle A_n(\mathbf{X}) | \hat{H} | A_n(\mathbf{X}) \rangle$$
 (11)

These excited state CMESs can be used in an ad hoc manner to perform MD simulations. The underlying assumption for these simulations is that the nuclear wave functions adiabatically maintain their excited state character during the dynamics and do not relax to the lower vibrational states. In the next section we will show that we can use them to obtain vibrational excited state absorption frequencies. For these frequency calculations, a natural question is that since we need to construct excited state CMESs, why don't we directly take the energy difference between CMESs energy minima to obtain the frequencies? We note that because of the requirement for the orthogonality to the lower states of the same expectation position, the "excited states" for CMESs do not rigorously correspond to the vibrational excited states solved from the Schrödinger equation, and therefore, the energy gaps between CMESs do not necessarily match well with the reference excited state absorption values. Additionally, the success of vibrational frequency calculations will demonstrate the good quality, at least near the equilibrium region, of the vibrational excited state CMESs, which we can use in the future to perform vibrationally excited state dynamics simulations.

Excited state CMES for harmonic oscillator model

The harmonic oscillator model was used to justify the use of classical MD to calculate vibrational spectra since its classical autocorrelation functions match exactly with the quantum autocorrelation functions in peak positions. Our group also showed that in the harmonic oscillator model, the ground state CMES differs from the underlying PES only by a universal shift of $\frac{1}{2}\hbar\omega^{59}$. Therefore, the classical dynamics picture remains the same, and CMES-MD is also exact for the harmonic oscillator⁵⁹. Here, to extend out CMES theory to excited states, we will analytically solve for the excited state CMESs for a harmonic oscillator and investigate their properties.

For the harmonic oscillator model $\hat{H} = \hat{p}^2/2m + m\omega^2(\hat{x} - x_e)^2/2$, it can be proven that the CMES ground state $|A_0(X)\rangle$ as a function of the expectation position X is the ground state of another harmonic oscillator $\hat{H}' = \hat{p}^2/2m + m\omega^2(\hat{x} - X)^2/2$, but with the center shifted to the nuclear expectation position X^{59} . Then the corresponding ground state CMES can be evaluated and gives

$$V_0^{\text{CMES}}(X) = \langle A_0(X) | \hat{H} | A_0(X) \rangle = \frac{1}{2} \hbar \omega + \frac{1}{2} m \omega^2 (X - x_e)^2.$$
 (12)

With the ground state $|A_0(X)\rangle$ obtained, we can employ Eq. 10 to solve the first excited state CMES analytically (see Supporting Information for details). The excited state wave function $A_1(x;X)$ is

$$A_1(x;X) = \psi_1^{\text{HO}}(x-X),$$
 (13)

where $\psi_n^{\text{HO}}(x-X)$ is the *n*th eigenfunction of a harmonic oscillator centered at X, and the corresponding CMES is

$$V_1^{\text{CMES}}(X) = \langle A_1(X) | \hat{H} | A_1(X) \rangle = \frac{3}{2} \hbar \omega + \frac{1}{2} m \omega^2 (X - x_e)^2.$$
 (14)

It can be seen that the wave function is the same as the first excited state wave function for

quantum harmonic oscillator except it is now centered at x = X. Furthermore, the excited state CMES is the same as the underlying harmonic PES but shifted up universally by $\frac{3}{2}\hbar\omega$, which is the quantum energy associated with the first excited state.

In fact, for the harmonic oscillator model, these elegant results can be generalized to even higher excited state CMESs with

$$V_n^{\text{CMES}}(X) = \langle A_n(X) | \hat{H} | A_n(X) \rangle = (n + \frac{1}{2})\hbar\omega + \frac{1}{2}m\omega^2(X - x_e)^2,$$
 (15)

which means that compared to the underlying harmonic PES, CMESs simply shift the energy universally up by $(n + 1/2)\hbar\omega$, the quantum energy for the *n*th state.

This universal shift does not change the shape of the effective potential and also does not change the classical dynamics picture. Therefore, the position autocorrelation functions remain the same for every excited state CMES:⁶⁴

$$\langle x(0)x(t)\rangle_n^{\text{CMES}} = \frac{kT}{m\omega^2}\cos\omega t,$$
 (16)

where the average $\langle \cdot \rangle$ is taken under the canonical ensemble. Furthermore, the Fourier transform of this autocorrelation function gives the same vibrational frequency ω as before. Despite the same frequency, we argue that because these dynamics simulations are performed on excited state CMESs and the underlying quantum picture corresponds to excited state harmonic oscillator wave functions, these vibrational frequencies ω should not be viewed as the fundamental transition frequency. Instead, they should be viewed as excited state absorption frequencies, which happen to be the same as the fundamental transition frequency in the harmonic oscillator model. This is the key hypothesis of this paper, which we will provide numerical support in "Results for anharmonic systems" section on a series of anharmonic model systems.

To further connect the classical autocorrelation functions with the quantum autocorrelation functions for excited state absorptions, here we consider a special ensemble for the harmonic oscillator, in which the ground state is not occupied whereas the excited states are occupied according to the Boltzmann distribution. In this special ensemble, since the ground state is not occupied, the quantum autocorrelation function contains information of excited state absorptions (mainly $1 \to 2$) but no fundamental transition. The position autocorrelation function can be computed analytically (see detailed derivation in Supporting Information):

$$\frac{1}{2}\langle \left[\hat{x}(0), \hat{x}(t)\right]_{+}\rangle = \frac{\hbar}{2m\omega} \frac{3 - e^{-\beta\hbar\omega}}{1 - e^{-\beta\hbar\omega}} \cos\omega t. \tag{17}$$

Obviously the Fourier transform of this quantum autocorrelation function still gives the frequency ω , but it should mainly be considered to correspond to the $1 \to 2$ transition. Comparing this quantum autocorrelation function with the classical autocorrelation function obtained from excited state CMES in Eq. 16, there is only a pre-factor difference, suggesting that it may be viable to use excited state CMES-MD to obtain excited state absorption spectra.

This argument can also be generalized to the $2 \to 3$ or even higher transitions by constructing other special ensembles, but the key hypothesis remains the same: since the classical autocorrelation function matches with the quantum autocorrelation function, we may use excited CMES-MD to obtain excited-state spectra.

Workflow

Based on the theory introduced above, here we present a detailed workflow for the construction of excited state CMESs.

- 1. For a given expectation position \mathbf{X} , solve the CMES ground state $|A_0(\mathbf{X})\rangle$ iteratively using Eq. 3 under the expectation position constraint ⁵⁹.
- 2. Evaluate the energy of $|A_0(\mathbf{X})\rangle$ to obtain the ground state CMES $V_0^{\text{CMES}}(\mathbf{X}) = \langle A_0(\mathbf{X})|\hat{H}|A_0(\mathbf{X})\rangle$.
- 3. At the same expectation position X, iteratively solve the constrained first CMES

excited state using Eq. 10:

$$\left(\hat{H} + \mathbf{f}_1(\mathbf{X}) \cdot \hat{\mathbf{x}} + g_{10} \cdot |A_0(\mathbf{X})\rangle \langle A_0(\mathbf{X})|\right) |A_1(\mathbf{X})\rangle = \tilde{E}(\mathbf{X})|A_1(\mathbf{X})\rangle$$
(18)

Note that ground state $|A_0(\mathbf{X})\rangle$ solved in step 1 is used here for the orthogonality constraint.

- 4. Evaluate the energy of $|A_1(\mathbf{X})\rangle$ to obtain the first excited state CMES $V_1^{\text{CMES}}(\mathbf{X}) = \langle A_1(\mathbf{X})|\hat{H}|A_1(\mathbf{X})\rangle$.
- 5. If needed, at the same expectation position **X**, iteratively solve higher CMES excited states and energies using Eq. 10. Note that lower energy CMES states are needed for the orthogonality constraints.
- 6. The step 1-5 can be repeated for any expectation position. Then energies with the same quantum number n but different expectation positions can be joint together and form the nth excited state CMES.
- 7. With numerical procedures, the minimum of each excited state CMES can be located and the Hessian matrix around the minimum can be constructed, which gives frequency information after diagonalization.

Results for anharmonic systems

To go beyond the simple harmonic oscillator model, here we test our proposed method on a series of anharmonic model systems. Note that conventional MD has only one PES and cannot construct vibrational excited state surface. Therefore, we can only obtain the same frequency for both $0 \to 1$ fundamental transition and any other $n \to n+1$ excited state transitions. In contrast, in the CMES-MD framework, we can use MD on the ground state CMES to obtain $0 \to 1$ transition frequencies, use MD on the first excited CMES to obtain

 $1 \rightarrow 2$ transitions, and so forth. We note that although MD results depend on the simulation temperature, this temperature effect is relatively small in the temperature range that most chemists care about. Therefore, in this paper, we will simply focus on the zero-temperature limit and only use their second-order derivative information to approximate the vibrational transition energies. However, we can always slightly go beyond this harmonic hessian approximation by running MD trajectories upon CMESs, which will sample anharmonic region on CMESs through elevated temperature. We will provide results for the Morse potential, quartic potential, double-well potential, and 2D anharmonic potential, all of which are important model systems for modeling practical chemical problems. The quantum results are used as reference, which are obtained either analytically or numerically with a dense grid.

Morse potential

The Morse potential is a typical model for bond vibrations. It has analytic quantum solutions, and the anharmonicity makes excited state transitions different from the $0 \to 1$ fundamental transition. Here we will test our method on the 1-D Morse potential with the form $V(x) = D_{\rm e}({\rm e}^{-2\alpha(x-x_{\rm e})} - 2{\rm e}^{-\alpha(x-x_{\rm e})})$, in which $D_{\rm e} = hc\omega_{\rm e}\chi_{\rm e}^2/(4\omega_{\rm e}\chi_{\rm e})$ and $\alpha = \sqrt{2\mu\hbar c\omega_{\rm e}\chi_{\rm e}}/\hbar$. Three parameters, $x_{\rm e}$, $\chi_{\rm e}$, and $\omega_{\rm e}$ completely determine the Morse potential, but we will not scan all these parameters due to the large computational expense. Instead, we select a few parameter sets that mimic real chemical bond vibrations for testing.

The first group of bonds is H-X bonds, where X can be C, N, or O. This group of bonds is of particular interest because they are known to be highly anharmonic. In the existing literature⁷⁷, there are Morse parameter sets fitted for these H-X bonds based on diatomic results (listed in Table S1). We observed that in these Morse potential parameter sets, different H-X diatomic molecules tend to have similar χ_e and x_e values, but their ω_e values can vary significantly. Therefore, we fix the value of χ_e to be 0.023 and the value of x_e to be 1.0 Å, and only scan the value of ω_e in the range from 2000 cm⁻¹ to 4000 cm⁻¹ to model the H-X vibrations in different chemical environments. The reduced mass is approximated to be the

mass of a hydrogen atom. We limit our discussions to $0 \to 1$, $1 \to 2$, and $2 \to 3$ transitions since the lowest few states are the most important. Therefore, we construct the ground, first excited, and second excited state CMESs using Eq. 3 and Eq. 10. Since we are focusing on the zero-temperature limit, we numerically obtain the second-order derivatives around the minima of each CMES to approximate the vibrational frequencies with the harmonic approximation. We will use the exact analytic quantum results as references, and we will also compare our results with the harmonic approximation results from the PES, which are nothing but ω_e for Morse potentials.

Figure 1 shows the ground state, first excited state, and second excited state CMESs for $\omega_{\rm e} = 3500\,{\rm cm^{-1}}$. In addition to the relative energy difference, we also note that their energy minima correspond to different nuclear positions, which essentially indicates that the bond length will grow as the system is excited. Furthermore, these energy curves no longer differ by a universal shift and thus will give different vibrational frequencies.

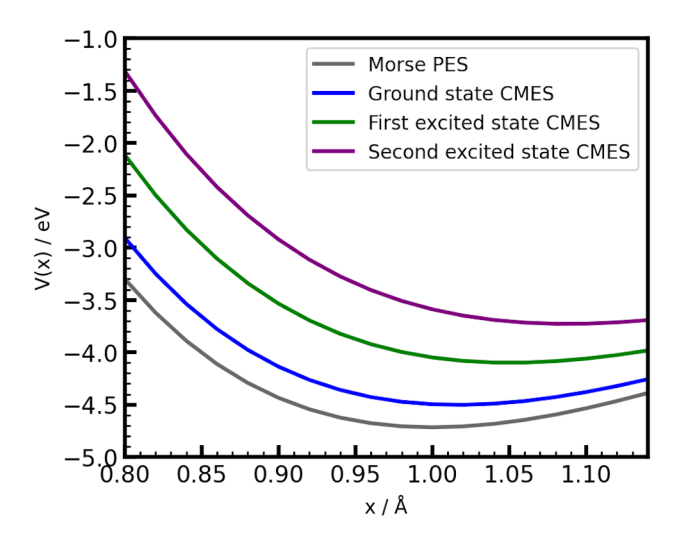


Figure 1: PES and ground and excited state CMESs for a 1D Morse potential. The parameters of the Morse potential are $\chi_e = 0.023$, $x_e = 1.0 \,\text{Å}$, and $\omega_e = 3500 \, \text{cm}^{-1}$

Figure 2 shows the CMES results for estimating the $0 \to 1$, $1 \to 2$, and $2 \to 3$ transition frequencies. For the $0 \to 1$ fundamental frequencies (panel a), the CMES harmonic approximation results excellently agree with the quantum reference results, with a percentage error of about 1%, whereas using the PES, the error is about 5%. These results are consistent

with results from the previous paper by two of us⁵⁹, where we found that CMES-MD can significantly outperform conventional MD in predicting fundamental frequencies. For the $1 \to 2$ transitions (panel b), the excited state CMES gives lower vibrational frequencies than those obtained from the ground state CMES. This trend is in very good agreement with the quantum reference results, where the $1 \to 2$ energy gap is smaller than the $0 \to 1$ energy gap due to anharmonicity. The percentage error is about 2%, which is slightly larger than that for the $0 \to 1$ fundamental transition. In contrast, the harmonic approximation based on the PES gives the same vibrational frequencies as the fundamental transitions and deviates more severely from the quantum reference. The story for the $2 \to 3$ transitions (panel c) is very similar: although the harmonic approximation based on the CMES gives a larger percentage error (around 5%) than in the $0 \to 1$ and $1 \to 2$ cases, it captures the decreasing trend of the energy gap and significantly outperforms the harmonic approximation results based on the original PES.

To further investigate the performance of our method in more general bond stretch cases, we next choose the Morse potential parameter sets for the diatomic F-F, O=O, and N=N molecules⁷⁷. These three diatomic molecules are good representatives of bond stretches for single bonds, double bonds, and triple bonds respectively. The parameters used are taken from reference⁷⁷ and are listed in Table S1 of the Supporting Information. The results for these systems are shown in Figure 3. We again see that our CMES-based method significantly outperforms the conventional PES-based method for all $0 \to 1$, $1 \to 2$, and $2 \to 3$ transitions.

Double-well and quartic potential

Next we apply our method to the more challenging double-well and quartic potential systems, which both share the potential form of $V(x) = ax^2 + bx^4$. The parameter b is always positive. When a is negative, the potential corresponds to a double-well potential; when a is zero, there is no second order term and the potential is quartic; and when a is positive, it is a symmetric

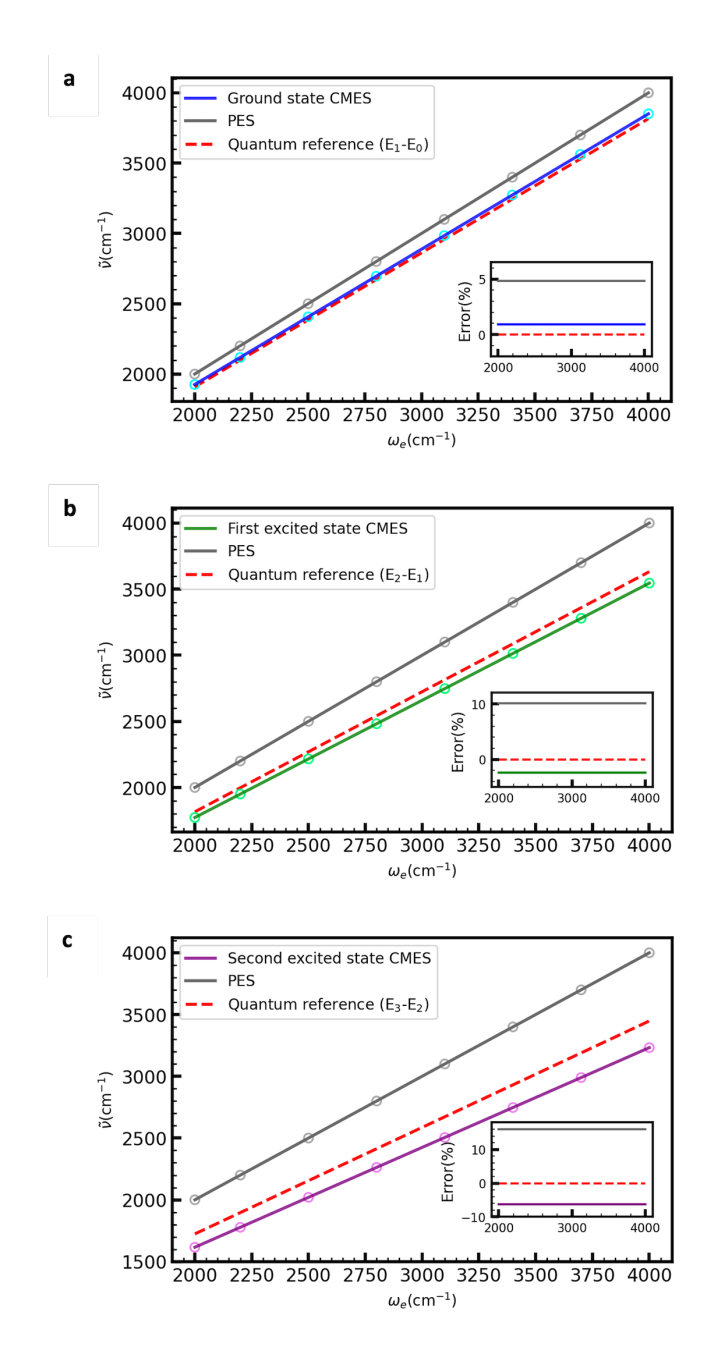


Figure 2: Transition frequencies from harmonic approximation using CMESs (colored solid lines) and PESs (grey solid lines) for (a) the fundamental $0 \to 1$ transition; (b) the $1 \to 2$ transition; and (c) the $2 \to 3$ transition. The red dashed lines are the exact quantum references. Based on the harmonic approximation, our CMES-based method greatly outperforms the conventional PES-based method.

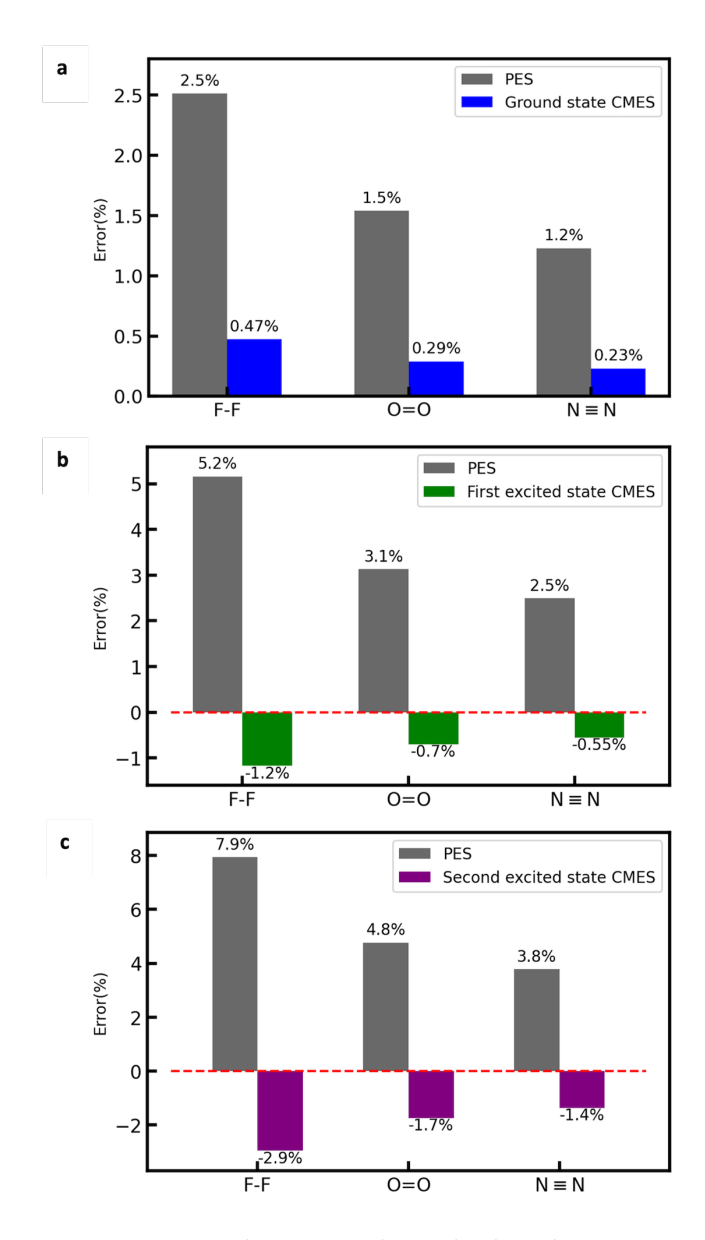


Figure 3: Relative percentage error between the calculated transition frequencies and the quantum references of F–F, O=O, N=N bonds for (a) the fundamental $0 \to 1$ transition; (b) the $1 \to 2$ transition; and (c) the $2 \to 3$ transition. Results using CMESs are colored and results using PESs are in grey. These results show that based on the harmonic approximation, our CMES-based method greatly outperforms the conventional method, yielding a much smaller percentage error.

single well potential with anharmonicity arising from the quartic bx^4 term. Figure 4 shows the ground and the first excited state CMESs for these three scenarios. For quantitative testing, we fix the value of b to be $32\,\mathrm{eV/\mathring{A}^4}$ and vary a from $-8\,\mathrm{eV/\mathring{A}^2}$ to $12\,\mathrm{eV/\mathring{A}^2}$. The results for the $0\to 1$ and $1\to 2$ transitions are shown in Figure 5, panel (a) and (b), respectively.

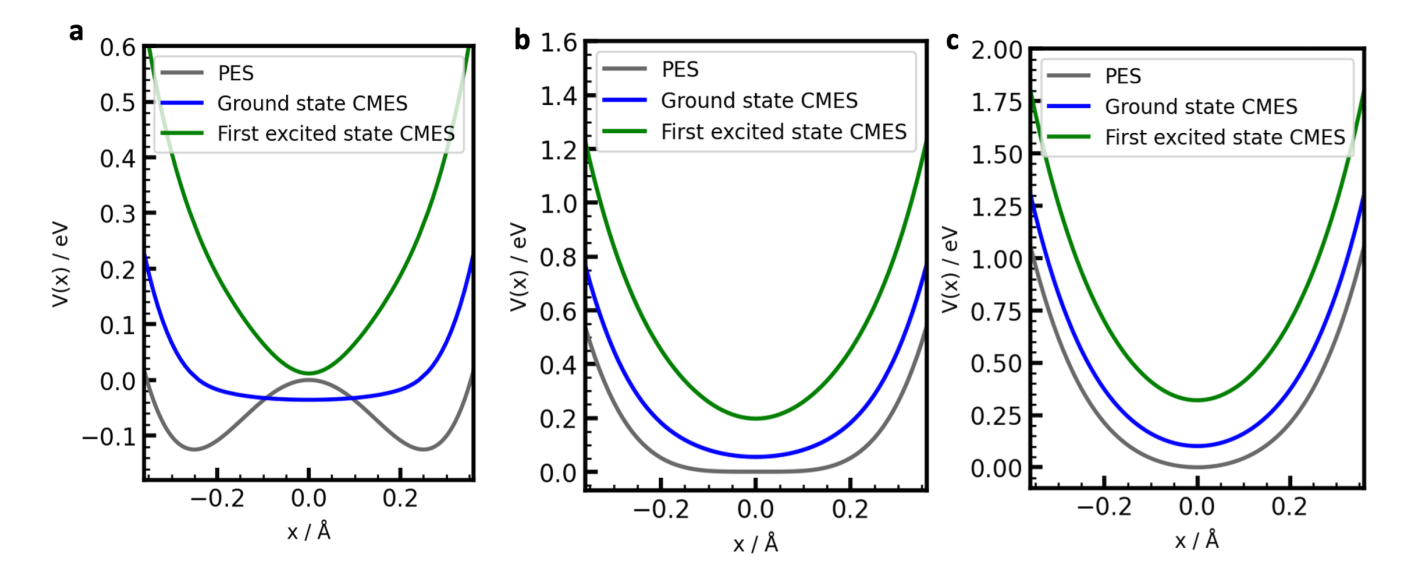


Figure 4: PES, ground state CMES, and first excited state CMES for model potential $V(x) = ax^2 + bx^4$. The parameter a varies with (a) $a = -4 \,\mathrm{eV/\mathring{A}}^2$; (b) $a = 0 \,\mathrm{eV/\mathring{A}}^2$; and (c) $a = 4 \,\mathrm{eV/\mathring{A}}^2$. The parameter b is set to be $32 \,\mathrm{eV/\mathring{A}}^4$ in all three cases.

In the double well region where a is negative, the barrier decreases as a becomes less negative, making the $0 \to 1$ tunnelling splitting increase as seen in the quantum reference. This trend can be captured by the harmonic results based on the ground state CMES, although we note that in the deep-tunneling region where a is highly negative, the CMES could have small absolute errors but large relative errors due to the tiny tunneling frequency. In contrast, conventional classical treatment based on the PES cannot describe tunneling, and at the zero-temperature limit, the particle always becomes trapped on either side of the well, leading to generally overestimated frequencies. Additionally, because of the incorrect physical picture, the increasing trend of the transition frequency when a is less negative is completely missed. For the $1 \to 2$ transition, the energy gap generally decreases as a becomes

less negative but turns flat and begins to increase when it is about $-4 \,\mathrm{eV/\AA^4}$. This qualitative picture can be captured by our method based on the first excited state CMES, although we note that the quantitative agreement is not completely satisfactory, especially when a is a very negative number, where CMES-MD could overestimate the gap by around 100%. For the conventional classical treatment, although it quantitatively slightly outperforms CMES-MD in most of the double-well excited state region with the grey curve being closer to the red curve than the green curve, we note that it does not mean that conventional MD is better since its underlying trapped-particle picture is completely unphysical.

For the quartic potential with a being zero, CMES results still have an excellent agreement with the quantum reference for the $0 \to 1$ transition. For the $1 \to 2$ transition, its quantitative error is significantly reduced compared to that in the double-well case. In contrast, since there is no harmonic term, the classical treatment with the harmonic approximation gives a zero frequency result, which is unphysical.

For cases with a greater than zero, the potential is an anharmonic single well potential. In this case, both the $0 \to 1$ and $1 \to 2$ energy gaps increase as a increases. This relatively easy trend can be captured by both our CMES-based method and the conventional PES-based method. However, our method outperforms the conventional method with a significantly better agreement with the quantum references. In the large a limit, the quartic terms can be ignored and the potential essentially becomes a harmonic oscillator. According to the previous discussions on the harmonic oscillator, both the $0 \to 1$ and $1 \to 2$ gaps converge to the same value and all methods give the same and correct asymptotic result.

Anharmonic 2D model potential

In addition to the 1D model potentials tested above, here we further apply our method on an anharmonic 2D model potential. The model potential takes the form of

$$V(x,y) = a_x x^2 + b_x x^4 + a_y y^2 + b_y y^4 + c_1 xy + c_2 x^2 y,$$
(19)

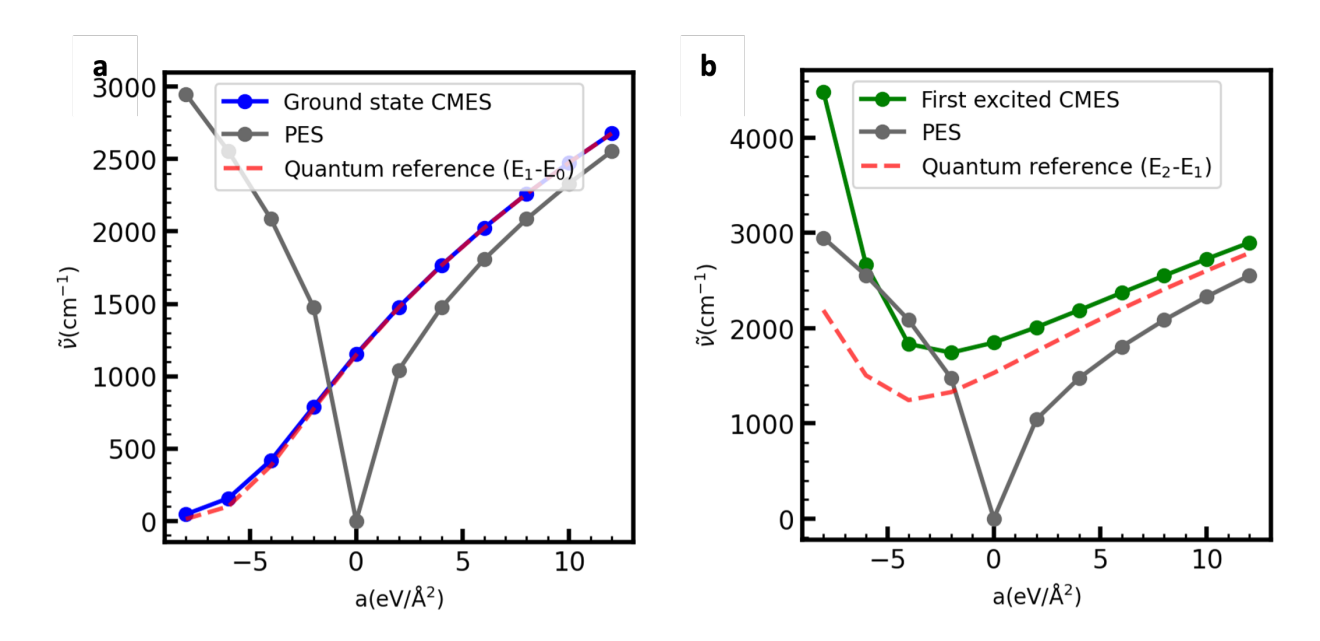


Figure 5: Transition frequencies from harmonic approximations using CMESs (colored solid lines) and PESs (grey solid lines) for model potential $V(x) = ax^2 + bx^4$ for (a) the $0 \to 1$ transition and (b) the $1 \to 2$ transition. The parameter b is fixed to $32 \, \text{eV/Å}^4$ and a is allowed to vary. Based on the harmonic approximation, our CMES-based method outperforms the conventional PES-based method with much better qualitative agreement with the quantum reference.

which includes both harmonic and quartic terms in both the x and y directions as well as the coupling terms xy and x^2y that couple the two directions.

We first set the potential to be $V(x,y) = 15x^2 + 30x^4 + 15y^2 + 20y^4 + 10xy + 30x^2y$. The quantum energy levels and the corresponding wavefunctions of this system can be obtained numerically by solving the Schrödinger equation. In the harmonic analysis, the two normal modes appear along the diagonal lines instead of along the x and y directions, due to the xy coupling term (see Supporting Information for contour plot of the potential). For this potential, the harmonic approximation gives $2332 \,\mathrm{cm}^{-1}$ and $3298 \,\mathrm{cm}^{-1}$ for the two modes, respectively, whereas the quantum references for the $(0,0) \rightarrow (0,1)$ and $(0,0) \rightarrow (1,0)$ fundamentals are $2383 \,\mathrm{cm}^{-1}$ and $3360 \,\mathrm{cm}^{-1}$, respectively. For higher excitations, $(0,1) \rightarrow (0,2)$ and $(1,0) \rightarrow (2,0)$, the reference frequencies are $2389 \,\mathrm{cm}^{-1}$ and $3370 \,\mathrm{cm}^{-1}$, respectively, indicating a relatively small $6-10 \,\mathrm{cm}^{-1}$ direct anharmonicity. However, the cross anharmonicity is as large as $100 \,\mathrm{cm}^{-1}$ with the reference frequencies for $(1,0) \rightarrow (1,1)$ and $(0,1) \rightarrow (1,1)$ being

 $2484 \,\mathrm{cm^{-1}}$ and $3461 \,\mathrm{cm^{-1}}$, respectively. The results of the CMES method together with the quantum references are shown in Figure 6(a). Note that we use the (m,n) CMES surface to obtain $(m,n) \to (m,n+1)$ and $(m,n) \to (m+1,n)$ excitation frequencies. We can see that all six transitions investigated here can be accurately predicted with the CMES method with largest errors being about $30 \,\mathrm{cm^{-1}}$. It is noteworthy that the large cross anharmonicty can be captured in this 2D model.

To further prove that the good results from the CMES method are not fortuitous, we construct another potential with stronger coupling: $V(x,y) = 15x^2 + 30x^4 + 15y^2 + 20xy$. Although the potential form appears simpler, its energy level picture is more complicated. The quantum references for the $(0,0)\rightarrow(0,1)$ and $(0,0)\rightarrow(1,0)$ fundamental frequencies are $1744\,\mathrm{cm^{-1}}$ and $3733\,\mathrm{cm^{-1}}$, respectively. Therefore, the $(0,0)\rightarrow(1,0)$ transition frequency is more than twice of that of $(0,0)\rightarrow(0,1)$ transition frequency, making the (0,2) state have lower energy than the (1,0) state. The energy ordering of the states for this potential as well as the CMES results are shown in Figure 6(b). Note that we have calculated more CMES states than the previous 2D potential to obtain more transition frequencies. We can see that even in this much more complicated case, the CMES method is again able to describe the vibrational frequencies reasonably well, especially for those transitions starting from relatively low-lying states. Anharmonicities and cross-anharmonicies are again accurately captured, indicating the validity of using CMES methods to describe both ground-state and excited-state absorptions.

Conclusions

In summary, we developed a procedure to calculate excited state CMESs and used them to obtain approximate vibrational excited state absorption frequencies. In the harmonic oscillator model, we showed that our CMES results are exact via analytical derivations. In the Morse potential model, our CMES-based method is highly accurate and significantly

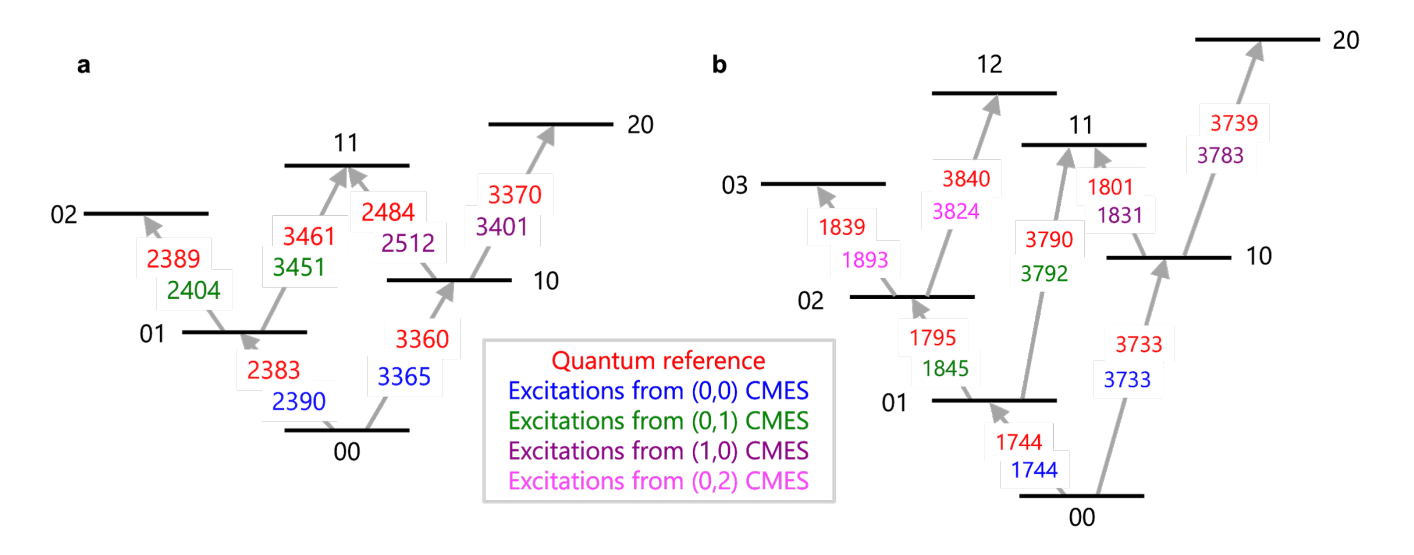


Figure 6: Transition frequencies (unit: cm⁻¹) from harmonic approximations using CMESs for model potential (a) $V(x,y) = 15x^2 + 30x^4 + 15y^2 + 20y^4 + 10xy + 30x^2y$ and (b) $V(x,y) = 15x^2 + 30x^4 + 15y^2 + 20xy$. Values in red are the quantum references, and values in blue, green, purple, and pink are the frequencies obtained from the (0,0), (0,1), (1,0), (0,2) CMES, respectively.

outperforms conventional PES-based harmonic approximation results. In the more challenging double-well potential and quartic potential, our method gives the correct physical picture and outperforms the conventional PES-based method. In the anharmonic 2D model potential, our CMES results accurately describe the excitations involving the two modes, and even capture cross anharmonicity. These results suggest the reliability of using excited state CMESs to describe vibrational excited state absorptions.

Finally, we note that the studies in this paper are all proof-of-principle model system tests, in which the underlying PES is known, and we can build ground and excited state CMESs on top of it. Although it seems that this procedure will no longer be practical for real systems because obtaining PESs is already computationally highly demanding and constructing CMESs is even more challenging, yet, fortunately, similar to the ground state CMES⁵⁹, which can be obtained from CNEO-DFT calculations ^{60–63}, we anticipate that excited state CMESs can be calculated with excited state CNEO methods, for example, CNEO time-dependent density functional theory (CNEO-TDDFT). The related method

development on CNEO-TDDFT is ongoing in our group, and this current paper on model systems serves as the theoretical motivation for its development. All these developments will make CNEO-based methods promising approaches for modeling and interpreting a variety of linear and nonlinear vibrational spectra.

Supporting Information Available

Detailed analytical derivations of excited state CMESs for harmonic oscillator; detailed derivation of time correlation function of harmonic oscillator in a special excited state ensemble; table for Morse potential parameters; and contour of wave functions for the anharmonic 2D model system.

Acknowledgment

We thank Nan Yang, Yuzhe Zhang, Yunrui Qiu, Xianyuan Zhao, and James Langford for helpful discussions. ChatGPT assisted with the editing of this manuscript. The authors are grateful for the funding support from the National Science Foundation under Grant 2238473 and from the University of Wisconsin via the Wisconsin Alumni Research Foundation.

References

- (1) Perakis, F.; De Marco, L.; Shalit, A.; Tang, F.; Kann, Z. R.; Kühne, T. D.; Torre, R.; Bonn, M.; Nagata, Y. Vibrational Spectroscopy and Dynamics of Water. *Chem. Rev.* **2016**, *116*, 7590–7607.
- (2) Wolke, C. T.; Fournier, J. A.; Dzugan, L. C.; Fagiani, M. R.; Odbadrakh, T. T.; Knorke, H.; Jordan, K. D.; McCoy, A. B.; Asmis, K. R.; Johnson, M. A. Spectroscopic Snapshots of the Proton-Transfer Mechanism in Water. *Science* 2016, 354, 1131–1135.

- (3) Yang, N.; Duong, C. H.; Kelleher, P. J.; McCoy, A. B.; Johnson, M. A. Deconstructing Water's Diffuse OH Stretching Vibrational Spectrum with Cold Clusters. *Science* **2019**, 364, 275–278.
- (4) Herzberg, G. Molecular Spectra and Molecular Structure. II, Infrared and Raman Spectra of Polyatomic Molecules; D. Van Nostrand Company: Toronto, 1945.
- (5) Baiz, C. R.; Błasiak, B.; Bredenbeck, J.; Cho, M.; Choi, J.-H.; Corcelli, S. A.; Dijkstra, A. G.; Feng, C.-J.; Garrett-Roe, S.; Ge, N.-H. et al. Vibrational Spectroscopic Map, Vibrational Spectroscopy, and Intermolecular Interaction. *Chem. Rev.* 2020, 120, 7152–7218.
- (6) Noda, I. Generalized Two-Dimensional Correlation Method Applicable to Infrared, Raman, and Other Types of Spectroscopy. Appl Spectrosc 1993, 47, 1329–1336.
- (7) Mukamel, S. *Principles of Nonlinear Optical Spectroscopy*; Oxford Series in Optical and Imaging Sciences; Oxford University Press: Oxford, New York, 1999.
- (8) Du, Q.; Superfine, R.; Freysz, E.; Shen, Y. R. Vibrational Spectroscopy of Water at the Vapor/Water Interface. *Phys. Rev. Lett.* **1993**, *70*, 2313–2316.
- (9) Dong, P.-T.; Cheng, J.-X. Pump–Probe Microscopy: Theory, Instrumentation, and Applications. *Spectroscopy* **2017**, *32*, 24–36.
- (10) Garrett-Roe, S.; Perakis, F.; Rao, F.; Hamm, P. Three-Dimensional Infrared Spectroscopy of Isotope-Substituted Liquid Water Reveals Heterogeneous Dynamics. J. Phys. Chem. B 2011, 115, 6976–6984.
- (11) Ashihara, S.; Huse, N.; Espagne, A.; Nibbering, E. T. J.; Elsaesser, T. Vibrational Couplings and Ultrafast Relaxation of the O-H Bending Mode in Liquid H2O. Chem. Phys. Lett. 2006, 424, 66-70.

- (12) Hamm, P.; Zanni, M. Concepts and Methods of 2D Infrared Spectroscopy; Cambridge University Press, 2011.
- (13) Khalil, M.; Demirdöven, N.; Tokmakoff, A. Coherent 2D IR Spectroscopy: Molecular Structure and Dynamics in Solution. *J. Phys. Chem. A* **2003**, *107*, 5258–5279.
- (14) Asbury, J. B.; Steinel, T.; Stromberg, C.; Corcelli, S. A.; Lawrence, C. P.; Skinner, J. L.; Fayer, M. D. Water Dynamics: Vibrational Echo Correlation Spectroscopy and Comparison to Molecular Dynamics Simulations. J. Phys. Chem. A 2004, 108, 1107– 1119.
- (15) Hamm, P.; Lim, M.; Hochstrasser, R. M. Structure of the Amide I Band of Peptides Measured by Femtosecond Nonlinear-Infrared Spectroscopy. J. Phys. Chem. B 1998, 102, 6123–6138.
- (16) Cho, M. Two-Dimensional Optical Spectroscopy; CRC press, 2009.
- (17) Petti, M. K.; Lomont, J. P.; Maj, M.; Zanni, M. T. Two-Dimensional Spectroscopy Is Being Used to Address Core Scientific Questions in Biology and Materials Science. J. Phys. Chem. B 2018, 122, 1771–1780.
- (18) Wilson, E. B., Jr.; Decius, J. G.; Cross, P. G. *Molecular Vibrations*; McGrow-Hill Book Company, Inc.: New York, 1955; Vol. 23.
- (19) Alecu, I. M.; Zheng, J.; Zhao, Y.; Truhlar, D. G. Computational Thermochemistry: Scale Factor Databases and Scale Factors for Vibrational Frequencies Obtained from Electronic Model Chemistries. J. Chem. Theory Comput. 2010, 6, 2872–2887.
- (20) Nielsen, H. H. The Vibration-Rotation Energies of Molecules. Rev. Mod. Phys. 1951, 23, 90–136.
- (21) Willetts, Andrew.; Handy, N. C.; Green, W. H.; Jayatilaka, Dylan. Anharmonic Corrections to Vibrational Transition Intensities. J. Phys. Chem. 1990, 94, 5608–5616.

- (22) Barone, V. Vibrational Zero-Point Energies and Thermodynamic Functions beyond the Harmonic Approximation. *J. Chem. Phys.* **2004**, *120*, 3059–3065.
- (23) Barone, V.; Biczysko, M.; Bloino, J. Fully Anharmonic IR and Raman Spectra of Medium-Size Molecular Systems: Accuracy and Interpretation. Phys. Chem. Chem. Phys. 2014, 16, 1759–1787.
- (24) Barone, V. Anharmonic Vibrational Properties by a Fully Automated Second-Order Perturbative Approach. J. Chem. Phys. 2004, 122, 014108.
- (25) Carpenter, W. B.; Yu, Q.; Hack, J. H.; Dereka, B.; Bowman, J. M.; Tokmakoff, A. Decoding the 2D IR Spectrum of the Aqueous Proton with High-Level VSCF/VCI Calculations. J. Chem. Phys. 2020, 153, 124506.
- (26) Hanson, M. D.; Readnour, J. A.; Hassanali, A. A.; Corcelli, S. A. Coupled Local-Mode Approach for the Calculation of Vibrational Spectra: Application to Protonated Water Clusters. J. Phys. Chem. Lett. 2021, 12, 9226–9232.
- (27) Shin, J.-W.; Hammer, N. I.; Diken, E. G.; Johnson, M. A.; Walters, R. S.; Jaeger, T. D.; Duncan, M. A.; Christie, R. A.; Jordan, K. D. Infrared Signature of Structures Associated with the H+(H2O)n (n = 6 to 27) Clusters. *Science* **2004**, *304*, 1137–1140.
- (28) Zeng, H. J.; Johnson, M. A. Demystifying the Diffuse Vibrational Spectrum of Aqueous Protons Through Cold Cluster Spectroscopy. *Annu. Rev. Phys. Chem.* **2021**, *72*, 667–691.
- (29) Zhang, Y.; Xu, X.; Yang, N.; Chen, Z.; Yang, Y. Describing Proton Transfer Modes in Shared Proton Systems with Constrained Nuclear-Electronic Orbital Methods. ChemRxiv 2023,
- (30) McDonald, D. C. I.; Wagner, J. P.; McCoy, A. B.; Duncan, M. A. Near-Infrared

- Spectroscopy and Anharmonic Theory of Protonated Water Clusters: Higher Elevations in the Hydrogen Bonding Landscape. *J. Phys. Chem. Lett.* **2018**, *9*, 5664–5671.
- (31) Yu, Q.; Bowman, J. M.; Fortenberry, R. C.; Mancini, J. S.; Lee, T. J.; Crawford, T. D.; Klemperer, W.; Francisco, J. S. Structure, Anharmonic Vibrational Frequencies, and Intensities of NNHNN+. J. Phys. Chem. A 2015, 119, 11623–11631.
- (32) Bowman, J. M. The Self-Consistent-Field Approach to Polyatomic Vibrations. *Acc. Chem. Res.* **1986**, *19*, 202–208.
- (33) Carter, S.; Culik, S. J.; Bowman, J. M. Vibrational Self-Consistent Field Method for Many-Mode Systems: A New Approach and Application to the Vibrations of CO Adsorbed on Cu(100). J. Chem. Phys. 1997, 107, 10458–10469.
- (34) Hammer, N. I.; Diken, E. G.; Roscioli, J. R.; Johnson, M. A.; Myshakin, E. M.; Jordan, K. D.; McCoy, A. B.; Huang, X.; Bowman, J. M.; Carter, S. The Vibrational Predissociation Spectra of the H5O2+●RGn(RG=Ar,Ne) Clusters: Correlation of the Solvent Perturbations in the Free OH and Shared Proton Transitions of the Zundel Ion. *J. Chem. Phys.* **2005**, *122*, 244301.
- (35) Bowman, J. M.; Carrington, T.; Meyer, H.-D. Variational Quantum Approaches for Computing Vibrational Energies of Polyatomic Molecules. Mol. Phys. 2008, 106, 2145— 2182.
- (36) Tuckerman, M. E.; Martyna, G. J. Understanding Modern Molecular Dynamics: Techniques and Applications. J. Phys. Chem. B 2000, 104, 159–178.
- (37) Tuckerman, M. E. Ab Initio Molecular Dynamics: Basic Concepts, Current Trends and Novel Applications. J. Phys.: Condens. Matter 2002, 14, R1297.
- (38) Iftimie, R.; Minary, P.; Tuckerman, M. E. Ab Initio Molecular Dynamics: Concepts, Recent Developments, and Future Trends. *Proc. Natl. Acad. Sci* **2005**, *102*, 6654–6659.

- (39) Karplus, M.; Porter, R. N.; Sharma, R. D. Dynamics of Reactive Collisions: The H+H2 Exchange Reaction. J. Chem. Phys. **2004**, 40, 2033–2034.
- (40) Noid, D. W.; Koszykowski, M. L.; Marcus, R. A. A Spectral Analysis Method of Obtaining Molecular Spectra from Classical Trajectories. J. Chem. Phys. 1977, 67, 404–408.
- (41) Swimm, R. T.; Delos, J. B. Semiclassical Calculations of Vibrational Energy Levels for Nonseparable Systems Using the Birkhoff–Gustavson Normal Form. J. Chem. Phys. 2008, 71, 1706–1717.
- (42) Yamada, T.; Aida, M. Fundamental Absorption Frequencies and Mean Structures at Vibrational Ground State from Quasi-Classical Direct Ab Initio MD: Triatomic Molecule. Chem. Phys. Lett. 2008, 452, 315–320.
- (43) Yamada, T.; Aida, M. Structures of Molecules in Ground and Excited Vibrational States from Quasiclassical Direct Ab Initio Molecular Dynamics. J. Phys. Chem. A 2010, 114, 6273–6283.
- (44) Guo, Y.; Thompson, D. L.; Sewell, T. D. Analysis of the Zero-point Energy Problem in Classical Trajectory Simulations. *J. Chem. Phys.* **1996**, *104*, 576–582.
- (45) Ben-Nun, M.; Levine, R. D. On the Zero Point Energy in Classical Trajectory Computations. J. Chem. Phys. 1996, 105, 8136–8141.
- (46) Cao, J.; Voth, G. A. The Formulation of Quantum Statistical Mechanics Based on the Feynman Path Centroid Density. II. Dynamical Properties. J. Chem. Phys. 1994, 100, 5106–5117.
- (47) Jang, S.; Voth, G. A. A Derivation of Centroid Molecular Dynamics and Other Approximate Time Evolution Methods for Path Integral Centroid Variables. J. Chem. Phys. 1999, 111, 2371–2384.

- (48) Craig, I. R.; Manolopoulos, D. E. Quantum Statistics and Classical Mechanics: Real Time Correlation Functions from Ring Polymer Molecular Dynamics. J. Chem. Phys. 2004, 121, 3368–3373.
- (49) Rossi, M.; Ceriotti, M.; Manolopoulos, D. E. How to Remove the Spurious Resonances from Ring Polymer Molecular Dynamics. *J. Chem. Phys.* **2014**, *140*, 234116.
- (50) Trenins, G.; Willatt, M. J.; Althorpe, S. C. Path-Integral Dynamics of Water Using Curvilinear Centroids. *J. Chem. Phys.* **2019**, *151*, 054109.
- (51) Feynman, R. P.; Hibbs, A. R.; Styer, D. F. Quantum Mechanics and Path Integrals; Courier Corporation, 2010.
- (52) Paesani, F.; Voth, G. A. A Quantitative Assessment of the Accuracy of Centroid Molecular Dynamics for the Calculation of the Infrared Spectrum of Liquid Water. J. Chem. Phys. 2010, 132, 014105.
- (53) Habershon, S.; Fanourgakis, G. S.; Manolopoulos, D. E. Comparison of Path Integral Molecular Dynamics Methods for the Infrared Absorption Spectrum of Liquid Water. J. Chem. Phys. 2008, 129, 074501.
- (54) Meyer, H. D.; Manthe, U.; Cederbaum, L. S. The Multi-Configurational Time-Dependent Hartree Approach. *Chem. Phys. Lett.* **1990**, *165*, 73–78.
- (55) Beck, M. H.; Jäckle, A.; Worth, G. A.; Meyer, H. D. The Multiconfiguration Time-Dependent Hartree (MCTDH) Method: A Highly Efficient Algorithm for Propagating Wavepackets. Phys. Rep. 2000, 324, 1–105.
- (56) Vendrell, O.; Gatti, F.; Lauvergnat, D.; Meyer, H.-D. Full-Dimensional (15-Dimensional) Quantum-Dynamical Simulation of the Protonated Water Dimer. I. Hamiltonian Setup and Analysis of the Ground Vibrational State. The Journal of Chemical Physics 2007, 127, 184302.

- (57) Vendrell, O.; Gatti, F.; Meyer, H.-D. Full Dimensional (15-Dimensional) Quantum-Dynamical Simulation of the Protonated Water Dimer. II. Infrared Spectrum and Vibrational Dynamics. J. Chem. Phys. 2007, 127, 184303.
- (58) Schröder, M.; Gatti, F.; Lauvergnat, D.; Meyer, H.-D.; Vendrell, O. The Coupling of the Hydrated Proton to Its First Solvation Shell. *Nat Commun* **2022**, *13*, 6170.
- (59) Chen, Z.; Yang, Y. Incorporating Nuclear Quantum Effects in Molecular Dynamics with a Constrained Minimized Energy Surface. J. Phys. Chem. Lett. 2023, 14, 279–286.
- (60) Xu, X.; Yang, Y. Constrained Nuclear-Electronic Orbital Density Functional Theory: Energy Surfaces with Nuclear Quantum Effects. J. Chem. Phys. 2020, 152, 084107.
- (61) Xu, X.; Yang, Y. Full-Quantum Descriptions of Molecular Systems from Constrained Nuclear–Electronic Orbital Density Functional Theory. J. Chem. Phys. 2020, 153, 074106.
- (62) Xu, X.; Yang, Y. Molecular Vibrational Frequencies from Analytic Hessian of Constrained Nuclear–Electronic Orbital Density Functional Theory. J. Chem. Phys. **2021**, 154, 244110.
- (63) Xu, X.; Chen, Z.; Yang, Y. Molecular Dynamics with Constrained Nuclear Electronic Orbital Density Functional Theory: Accurate Vibrational Spectra from Efficient Incorporation of Nuclear Quantum Effects. J. Am. Chem. Soc. 2022, 144, 4039–4046.
- (64) Tuckerman, M. Statistical Mechanics: Theory and Molecular Simulation; Oxford university press, 2010.
- (65) Lu, D.-h.; Hase, W. L. Classical Mechanics of Intramolecular Vibrational Energy Flow in Benzene. IV. Models with Reduced Dimensionality. J. Chem. Phys. 1988, 89, 6723– 6735.

- (66) Corcelli, S. A.; Lawrence, C. P.; Skinner, J. L. Combined Electronic Structure/Molecular Dynamics Approach for Ultrafast Infrared Spectroscopy of Dilute HOD in Liquid H 2 O and D 2 O. J. Chem. Phys. **2004**, 120, 8107–8117.
- (67) Li, F.; Skinner, J. L. Infrared and Raman Line Shapes for Ice Ih. I. Dilute HOD in H 2 O and D 2 O. J. Chem. Phys. **2010**, 132, 204505.
- (68) Schmidt, J. R.; Roberts, S. T.; Loparo, J. J.; Tokmakoff, A.; Fayer, M. D.; Skinner, J. L. Are Water Simulation Models Consistent with Steady-State and Ultrafast Vibrational Spectroscopy Experiments? Chem. Phys. 2007, 341, 143–157.
- (69) Auer, B.; Kumar, R.; Schmidt, J. R.; Skinner, J. L. Hydrogen Bonding and Raman, IR, and 2D-IR Spectroscopy of Dilute HOD in Liquid D2O. Proc. Natl. Acad. Sci. 2007, 104, 14215–14220.
- (70) Schmidt, JR.; Corcelli, SA.; Skinner, JL. Pronounced Non-Condon Effects in the Ultrafast Infrared Spectroscopy of Water. J. Chem. Phys. 2005, 123, 044513.
- (71) Tan, J. A.; Kuo, J.-L. A Closer Examination of the Coupling between Ionic Hydrogen Bond (IHB) Stretching and Flanking Group Motions in (CH3OH)2H+: The Strong Isotope Effects. *Phys. Chem. Chem. Phys.* **2016**, *18*, 14531–14542.
- (72) Daly, C. A. J.; Streacker, L. M.; Sun, Y.; Pattenaude, S. R.; Hassanali, A. A.; Petersen, P. B.; Corcelli, S. A.; Ben-Amotz, D. Decomposition of the Experimental Raman and Infrared Spectra of Acidic Water into Proton, Special Pair, and Counterion Contributions. J. Phys. Chem. Lett. 2017, 8, 5246–5252.
- (73) Rey, R.; Møller, K. B.; Hynes, J. T. Hydrogen Bond Dynamics in Water and Ultrafast Infrared Spectroscopy. J. Phys. Chem. A 2002, 106, 11993–11996.
- (74) Auer, B. M.; Skinner, J. L. IR and Raman Spectra of Liquid Water: Theory and Interpretation. J. Chem. Phys. 2008, 128, 224511.

- (75) Dirac, P. A. M.; Bohr, N. H. D. The Quantum Theory of the Emission and Absorption of Radiation. *Proc. R. Soc. A* **1997**, *114*, 243–265.
- (76) Conte, R.; Aieta, C.; Botti, G.; Cazzaniga, M.; Gandolfi, M.; Lanzi, C.; Mandelli, G.; Moscato, D.; Ceotto, M. Anharmonicity and Quantum Nuclear Effects in Theoretical Vibrational Spectroscopy: A Molecular Tale of Two Cities. *Theor Chem Acc* 2023, 142, 53.
- (77) Huber, K.-P. Molecular Spectra and Molecular Structure: IV. Constants of Diatomic Molecules; Springer Science & Business Media, 2013.

TOC Graphic

